JOURNAL OF GUIDANCE, CONTROL, AND DYNAMICS
Vol. 39, No. 1, January 2016

Engineering Notes

Adaptive Postcapture Backstepping Control for Tumbling Tethered Space Robot–Target Combination

Panfeng Huang,* Dongke Wang,†
Zhongjie Meng,† and Fan Zhang†
Northwestern Polytechnical University, 710072 Xi'an, People's Republic of China
and
Jian Guo‡
Delft University of Technology, 2629 HS Delft, The Netherlands

DOI: 10.2514/1.G001309

Nomenclature

a	=	positive parameter
$[a_{tx} \quad a_{ty} \quad a_{tz}]^T$	=	linear acceleration due to the tether tension, m · s^{-2}
$[a_x \quad a_y \quad a_z]^T$	=	linear acceleration of the gripper's thruster force, m · s^{-2}
$C(k)$	=	matrix in coordinated desaturation controller
$\boldsymbol{d}$	=	position vector of the capture position, m
F_l	=	tether tension, N
I	=	inertia matrix of the combination, kg · m^2
I_0	=	nominal value of combination's inertia matrix, kg · m^2
K_ξ	=	positive-definite design matrix
k_2	=	positive-definite design matrix
m	=	mass of tethered space robot–target combination, kg
$Ox_l y_l z_l$	=	space tether frame
$Ox_p y_p z_p$	=	space platform orbital frame
$Ox_t y_t z_t$	=	combination orbital frame
$Ox_t' y_t' z_t'$	=	combination body frame
P	=	positive-definite design matrix
R	=	transformation matrix from platform orbital frame to combination body frame
$S(k)$	=	constant positive weighting matrix
$\boldsymbol{T}_l$	=	tether control torque, Nm
$[x \quad y \quad z]^T$	=	centroid position of the combination in the platform orbital frame, m
ΔI	=	inertia matrix uncertainty, kg · m^2
ε	=	positive parameter
$\boldsymbol{\lambda}(k)$	=	Lagrange multiplier
$\boldsymbol{\lambda}_L$	=	upper bound of disturbance
$\hat{\boldsymbol{\lambda}}_L$	=	estimation values of disturbance
μ	=	positive design parameter
$\boldsymbol{\xi}$	=	state of the auxiliary design system
$\boldsymbol{\sigma}$	=	modified Rodrigues parameters
$\boldsymbol{\sigma}_d$	=	desired modified Rodrigues parameters
$\boldsymbol{\tau}(k)$	=	vector of optimal thruster force and tether tension
$\boldsymbol{\tau}_c$	=	control torque of the combination, N · m
$\boldsymbol{\tau}_d$	=	disturbing torques, N · m
$\boldsymbol{\tau}_t$	=	control torque of the thruster, N · m
$\boldsymbol{\tau}_l$	=	control torque of the tether, N · m
$\boldsymbol{\omega}$	=	absolute angular velocity of the combination, rad · s^{-1}
$\boldsymbol{\omega}_d$	=	desired angular velocity of the combination, rad · s^{-1}

Received 9 February 2015; revision received 3 March 2015; accepted for publication 5 March 2015; published online 10 April 2015.

*Research Center for Intelligent Robotics, School of Astronautics; also National Key Laboratory of Aerospace Flight Dynamics (Corresponding Author).

†Research Center for Intelligent Robotics, School of Astronautics; also National Key Laboratory of Aerospace Flight Dynamics.

‡Faculty of Aerospace Engineering.

I. Introduction

TETHERED space robot (TSR) systems consist of a gripper, a space tether, and a space platform (Fig. 1) for future use in on-orbit services including on-orbit maintenance, on-orbit refueling, auxiliary orbit transfer, and space debris removal [1–2]. Many problems may arise during the different phases of a TSR capture mission, which is typically separated into the deployment, approach, capture, and postcapture phases. Research into the issues of deployment and capture control can be found in the literature [3–4].

The attitude control of a tethered system in space has received extensive attention, with several articles published on the subject in recent years. Nohmi [5] investigated the arm link to control the TSR's attitude during the deployment phase, and a microgravity experiment was conducted to validate the feasibility of this scheme. Godard [6] designed a nonlinear optimal controller using an inverse optimal technique to control the attitude of a satellite via tether offset variations. Bergamaschi and Bonon [7] studied the coupling between the tether taut string vibrations and the satellite attitude motion. Wang [8] proposed an attitude and orbit coordinated control method using a mobile tether attachment point for the tethered robot in the approaching phase.

The control of a traditional space robot has been studied by many researchers, and postcapture control is one of the main research problems. Yoshida [9] proposed a possible control sequence that included the bias momentum approach during the approaching phase, the impedance control during the impact phasem and the distributed momentum control during the postimpact phase for a successful capturing operation. Flores-Abad and Ma [10] proposed an optimal control strategy for a space manipulator to provide minimal impact to the base satellite during a capturing operation. Liu et al. [11] derived an impact model to simulate the postimpact dynamics of the entire systems and designed a proportional-derivative controller controller to maintain the stabilization of the robot system after the capture of the object. Aghili [12] focused on controlling the space manipulator in the postcapture phase to bring a tumbling satellite to rest. Xu et al. [13] proposed a method for berthing a target and reorientating the base using manipulator motion only after the capture.

After a target is captured by a TSR, the gripper and the target form a new combination system. The dynamic characteristics of the combination system differ from those of a TSR in its deployment, approach, or capture phase. Due to the presence of the space tether, the postcapture dynamic characteristics of the combination system can be distinguished from the aforementioned characteristics of a traditional space robot. The collision during the capture and the original target rotation lead to a tumbling of the combination, which

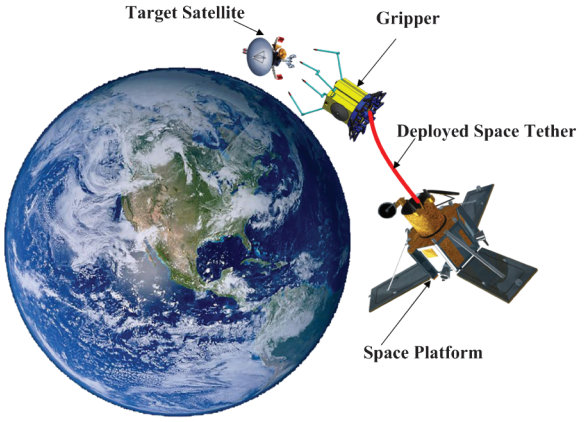

Fig. 1 TSR system.

could cause the tether to become tangled with the combination and influence the security of the space platform.

Compared with the combination system, the control torques provided by the thrusters of the TSR are usually limited. However, the saturation of the thruster during the combination stabilization may influence the attitude control of the combination, which was not considered in previous work [14].

The existence of input saturation can degrade the system control performance, and it even leads to the system instability. Therefore, several control methods have been proposed to deal with the systems with input saturation. In [15], command filters are presented to implement physical constraints on the virtual control laws, and the tedious analytic computations of time derivatives of virtual control laws are canceled. In [16], a robust adaptive controller is investigated for the longitudinal dynamics of a generic hypersonic flight vehicle and command filters are used to compensate the actuator of the hypersonic aircraft. By introducing auxiliary design systems to analyze the effect of input constraints, an adaptive neural network control with backstepping is proposed for surface ships with input saturation in [17]. In [18], a robust adaptive control was proposed based on the backstepping technique and the special property of a hyperbolic tangent function and a Nussbaum function are used to deal with the input saturation.

Besides, the disturbance including the inertia uncertainty and other attitude-disturbing torques may exert an influence on the performance of the combination attitude control. Given the problems mentioned previously, a robust adaptive backstepping controller is proposed to realize stabilization of a tumbling tethered space robot–target combination in this Note.

This Note consists of four main sections. Section II uses the Euler formulation approach to obtain the dynamic equations of motion for the combination system. In Sec. III, a robust adaptive controller is designed based on backstepping control and its stability is analyzed. Additionally, an optimal coordinated desaturation controller using a thruster and space tether is considered afterward. In Sec. IV, the feasibility of the robust adaptive backstepping control is validated using a numerical simulation and the results are presented and analyzed. The conclusions are discussed in Sec. V.

II. Dynamics Model

A. Task Description

As shown in Fig. 2, due to the spinning of the target and the collision between the gripper and a target, the gripper rotates along with the target after the capture, and the combination system consists of the gripper and the target. The origin of the space platform orbital frame $Ox_py_pz_p$ is located at the centroid of the space platform. The axes of the coordinate are oriented as follows: the x axis is in the orbital plane in the local horizontal direction, the y axis is along the orbital normal, and the z axis is collinear with a line that extends from the center of the Earth to the centroid of the space platform, and it completes a right-handed triad. Given the flying-around distance for the platform, observing the target before the capturing mission and the limited fuel for the gripper's thrusters in the capturing mission, the tether is assumed to be a few hundred meters long in this Note. Therefore, the $Ox_ty_tz_t$ denotes the combination orbital frame that is approximately parallel with $Ox_py_pz_p$. $Ox_ly_lz_l$ is the space tether frame with its x axis along the tether direction, and $Ox_t'y_t'z_t'$ is the combination body frame.

The following assumptions are made:

1) The tether is inelastic and massless.

2) The position and attitude of the space platform can be maintained during the coordinated attitude control of the combination system.

3) The target is not actuated.

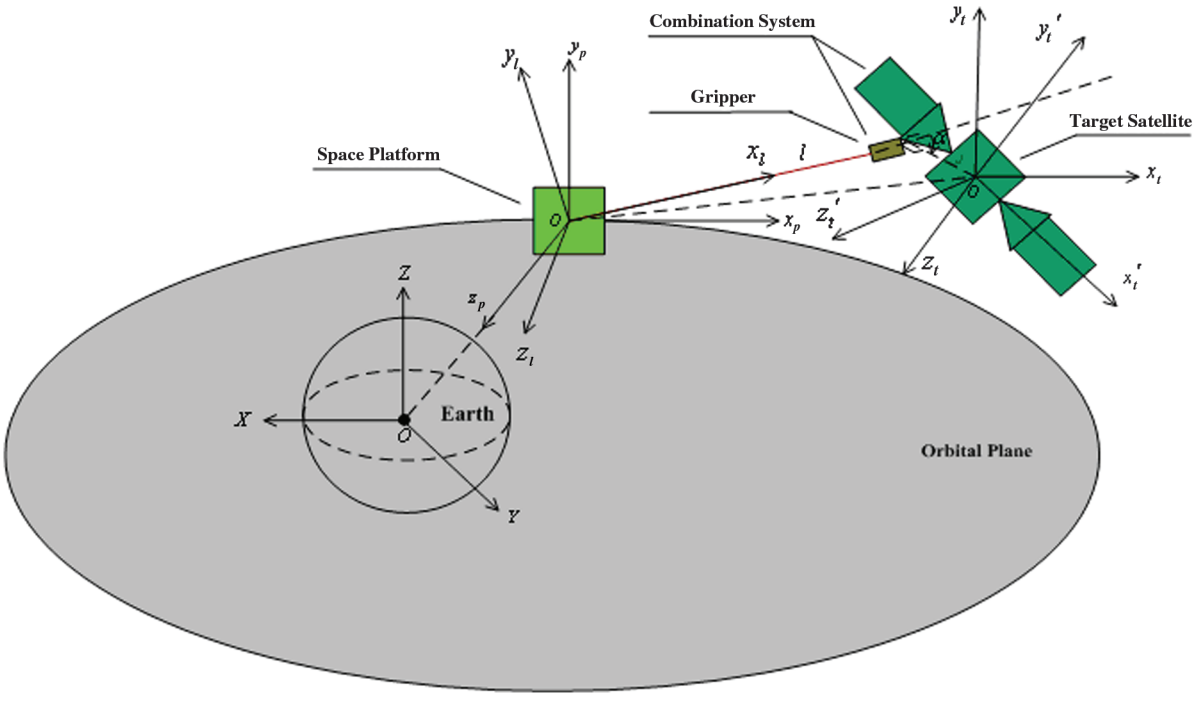

Fig. 2 Target capture of the TSR.

B. Attitude Dynamics Model

Assuming the combination system is a rigid body, its attitude dynamic equation can be given by the following equation:

$$I\dot{\boldsymbol{\omega}} = -\boldsymbol{\omega}^{\times} I\boldsymbol{\omega} + \boldsymbol{\tau}_c + \boldsymbol{\tau}_d \tag{1}$$

where $\boldsymbol{\omega} = [\,\omega_1 \quad \omega_2 \quad \omega_3\,]^T \in R^3$ denotes the absolute angular velocity of the combination expressed in $Ox_t'y_t'z_t'$; $I \in R^{3\times3}$ is the inertia matrix of the combination, where $I = I_0 + \Delta I$ (with I_0 as the nominal value and ΔI as the bounded uncertainty due to the thruster consumption and possible target parameter identification); $\boldsymbol{\tau}_c \in R^3$ denotes the control torque of the combination and can be expressed as $\boldsymbol{\tau}_c = \boldsymbol{\tau}_t + \boldsymbol{\tau}_l$, where $\boldsymbol{\tau}_t$ is the control torque of the thrusters on the gripper and equivalently realized via pulsewidth modulation (PWM) thrusters; $\boldsymbol{\tau}_l \in R^3$ denotes the control torque caused by tension along the space tether when the direction of tension does not go through the centroid of combination; $\boldsymbol{\omega}^{\times}$ is the skew-symmetric matrix of $\boldsymbol{\omega}$; and $\boldsymbol{\tau}_d \in R^3$ is the attitude disturbance torque.

The modified Rodrigues parameters [19] are adopted to describe the kinematics model of the combination attitude as follows:

$$\dot{\boldsymbol{\sigma}} = G(\boldsymbol{\sigma})\boldsymbol{\omega} \tag{2}$$

where $\boldsymbol{\sigma} = [\,\sigma_1 \quad \sigma_2 \quad \sigma_3\,]^T \in R^3$, and $G(\boldsymbol{\sigma})$ is defined as follows:

$$G(\boldsymbol{\sigma}) = \frac{1}{4}[(1-\boldsymbol{\sigma}^T\boldsymbol{\sigma})I_3 + 2\boldsymbol{\sigma}^{\times} + 2\boldsymbol{\sigma}\boldsymbol{\sigma}^T] \tag{3}$$

where I_3 is a 3×3 unit matrix.

The transformation matrix from the platform orbital frame to the combination body frame is

$$R = I_3 - \frac{4(1-\boldsymbol{\sigma}^2)}{(1+\boldsymbol{\sigma}^2)^2}[\boldsymbol{\sigma}^{\times}] + \frac{8}{(1+\boldsymbol{\sigma}^2)^2}[\boldsymbol{\sigma}^{\times}]^2 \tag{4}$$

III. Orbit Dynamic Model

The Hill equation is adopted to represent the orbit motion of the combination system:

$$\begin{cases} \ddot{x} - 2n\dot{z} = a_x + a_{tx} - n^2\varepsilon_x \\ \ddot{y} + n^2 y = a_y + a_{ty} - n^2\varepsilon_y \\ \ddot{z} + 2n\dot{x} - 3n^2 z = a_z + a_{tz} - n^2\varepsilon_z \end{cases} \tag{5}$$

where $[\,x \quad y \quad z\,]^T \in R^3$ is the centroid position of the combination in the platform orbital frame $Ox_py_pz_p$, and n denotes the mean orbital angular velocity. The linear acceleration of the gripper's thruster force is denoted by $[\,a_x \quad a_y \quad a_z\,]^T \in R^3$, and $[\,a_{tx} \quad a_{ty} \quad a_{tz}\,]^T \in R^3$ denotes the linear acceleration due to the tether tension.

Define the position vector of the capture position in the combination body frame as $\boldsymbol{d}$, and the tether tension as F_l, which satisfies $F_l \geq 0$. The tether tension vector in $Ox_py_pz_p$ can be written as

$$\boldsymbol{F} = -\frac{[x,y,z]^T + R^{-1}\mathrm{d}}{\|[x,y,z]^T + R^{-1}\mathrm{d}\|}F_l \tag{6}$$

By multiplying by the transformation matrix R, the tether force in the combination body frame can be obtained and the tether control torque can be acquired:

$$\boldsymbol{\tau}_l = \boldsymbol{d} \times (R\boldsymbol{F}) \tag{7}$$

IV. Coordinated Control Strategies

Given the thruster saturation and disturbance including the inertia uncertainty and other attitude-disturbing torque, a robust adaptive backstepping controller is proposed to realize stabilization of a tumbling tethered space robot–target combination in this section. Then, a stability analysis is carried out. Finally, an optimal coordinated controller is designed to further solve the problems of thruster saturation.

A. Robust Adaptive Attitude Control for Postcapture Combination

Step 1: Define the attitude error as $\boldsymbol{\sigma}_e = \boldsymbol{\sigma} - \boldsymbol{\sigma}_d$. The kinematics of the attitude error $\boldsymbol{\sigma}_e$ is written as:

$$\dot{\boldsymbol{\sigma}}_e = \dot{\boldsymbol{\sigma}} - \dot{\boldsymbol{\sigma}}_d = G(\boldsymbol{\sigma})\boldsymbol{\omega} - \dot{\boldsymbol{\sigma}}_d \tag{8}$$

Take the angular velocity of the combination $\boldsymbol{\omega}$ as the virtual control and design $\boldsymbol{\omega}_c$ as

$$\boldsymbol{\omega}_c = G^{-1}(\boldsymbol{\sigma})(-k_1\boldsymbol{\sigma}_e + \dot{\boldsymbol{\sigma}}_d) \tag{9}$$

where k_1 is a positive-definite design matrix.

Introduce a new state variable $\boldsymbol{\omega}_d$ that can be obtained by the following first-order filter:

$$\boldsymbol{\varepsilon}\dot{\boldsymbol{\omega}}_d + \boldsymbol{\omega}_d = \boldsymbol{\omega}_c, \qquad \boldsymbol{\omega}_d(0) = \boldsymbol{\omega}_c(0) \tag{10}$$

where $\boldsymbol{\varepsilon} > 0$.

Define $\boldsymbol{y} = \boldsymbol{\omega}_d - \boldsymbol{\omega}_c$ and $\boldsymbol{\omega}_e = \boldsymbol{\omega} - \boldsymbol{\omega}_d$; $\dot{\boldsymbol{\sigma}}_e$ can be rewritten as

$$\dot{\boldsymbol{\sigma}}_e = G(\boldsymbol{\sigma})(\boldsymbol{\omega}_e + \boldsymbol{y}) - k_1\boldsymbol{\sigma}_e \tag{11}$$

Step 2: The dynamics of the angular velocity error $\boldsymbol{\omega}_e$ is expressed as

$$I\dot{\boldsymbol{\omega}}_e = -\boldsymbol{\omega}^{\times} I\boldsymbol{\omega} - I\dot{\boldsymbol{\omega}}_d + \boldsymbol{\tau}_c + \boldsymbol{\tau}_d \tag{12}$$

To analyze the constraint effect of thruster saturation in this note, an auxiliary design system is given by

$$\dot{\boldsymbol{\xi}} = \begin{cases} -K_{\xi}\boldsymbol{\xi} - \frac{|\boldsymbol{\omega}_e^T(I^{-1}\Delta\boldsymbol{\tau}_c)| + 0.5(I^{-1}\Delta\boldsymbol{\tau}_c)^T(I^{-1}\Delta\boldsymbol{\tau}_c)}{\|\boldsymbol{\xi}\|^2}\boldsymbol{\xi} + (I^{-1}\Delta\boldsymbol{\tau}_c), & \|\boldsymbol{\xi}\| \geq \mu \\ 0, & \|\boldsymbol{\xi}\| < \mu \end{cases} \tag{13}$$

where $\boldsymbol{\xi}$ is the state of the auxiliary design system; $\Delta\boldsymbol{\tau}_c = \boldsymbol{\tau}_c - \boldsymbol{\tau}_{c0}$; μ is a small positive design parameter; and K_{ξ} is a positive-definite design matrix.

The control law is designed as

$$\boldsymbol{\tau}_{c0} = \boldsymbol{\omega}^{\times} I_0\boldsymbol{\omega} + I_0\dot{\boldsymbol{\omega}}_d - k_2(\boldsymbol{\omega}_e - \boldsymbol{\xi}) - PG(\boldsymbol{\sigma})\boldsymbol{\sigma}_e - \frac{\hat{\boldsymbol{\lambda}}_L\boldsymbol{\omega}_e}{|\boldsymbol{\omega}_e| + \varepsilon_{\lambda}} \tag{14}$$

where k_2 and P are positive-definite design matrices. To compensate the saturation of the thrusters, the state of the auxiliary design system $\boldsymbol{\xi}$ is involved in the control law [Eq. (14)]. Moreover, the disturbance of the attitude disturbing torques and inertia uncertainty may have influence on the performance of the combination attitude controller. Therefore, an adaptive control law $\hat{\boldsymbol{\lambda}}_L$ is designed to estimate the upper bound of the disturbance as follows:

The error dynamics of $\boldsymbol{\omega}_e$ can be expressed as

$$I\dot{\boldsymbol{\omega}}_e = -k_2(\boldsymbol{\omega}_e - \boldsymbol{\xi}) - PG(\boldsymbol{\sigma})\boldsymbol{\sigma}_e + \boldsymbol{\tau}_d - \boldsymbol{\omega}^{\times}\Delta I\boldsymbol{\omega} - \Delta I\dot{\boldsymbol{\omega}}_d \tag{15}$$

The term $\boldsymbol{\tau}_d - \boldsymbol{\omega}^{\times}\Delta I\boldsymbol{\omega} - \Delta I\dot{\boldsymbol{\omega}}_d$ is the corresponding disturbance. Assuming $\boldsymbol{\tau}_d$ and ΔI are bounded, then $\boldsymbol{\tau}_d - \boldsymbol{\omega}^{\times}\Delta I\boldsymbol{\omega} - \Delta I\dot{\boldsymbol{\omega}}_d$ is also bounded. Therefore, there exists a positive constant $\boldsymbol{\lambda}_L$ that satisfies $\|\boldsymbol{\tau}_d - \boldsymbol{\omega}^{\times}\Delta I\boldsymbol{\omega} - \Delta I\dot{\boldsymbol{\omega}}_d\| \leq \|\boldsymbol{\lambda}_L\|$. Define $\hat{\boldsymbol{\lambda}}_L$ as the estimation values, and the adaptive law of $\hat{\boldsymbol{\lambda}}_L$ is given by

$$\dot{\hat{\boldsymbol{\lambda}}}_L = \frac{a\boldsymbol{\omega}_e * \boldsymbol{\omega}_e}{|\boldsymbol{\omega}_e| + \varepsilon_{\lambda}} \tag{16}$$

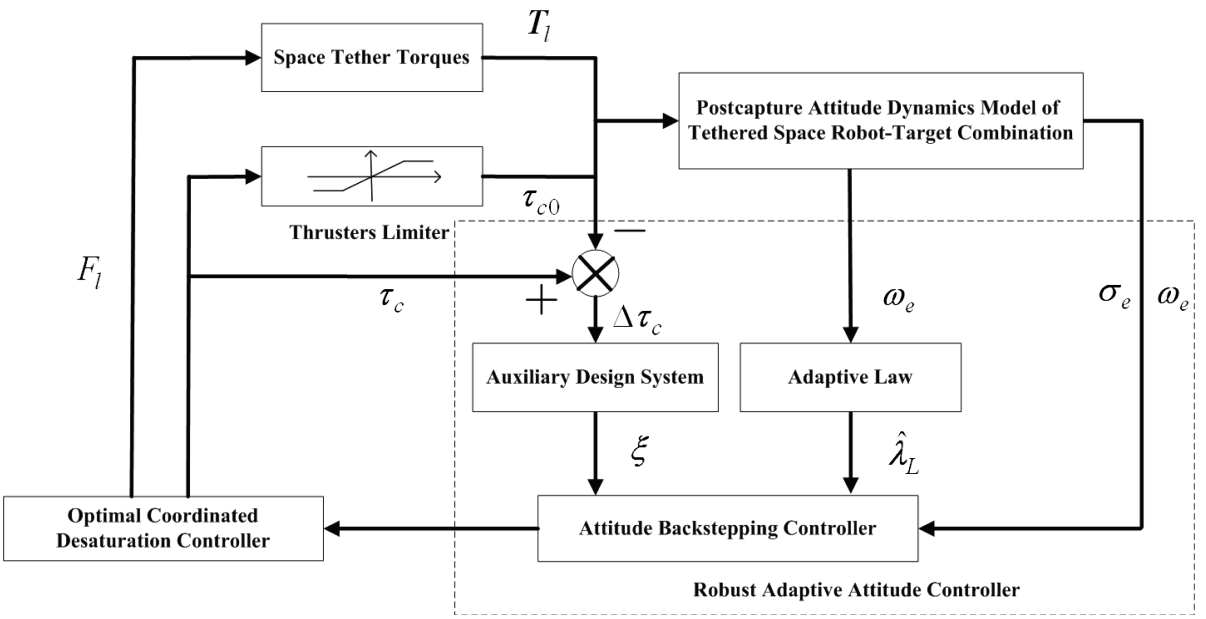

Fig. 3 Block diagram of the robust adaptive backstepping attitude controller.

where a and ε are positive parameters, and $\boldsymbol{\omega}_e * \boldsymbol{\omega}_e \triangleq (\omega_{e1}\omega_{e2} \quad \omega_{e2}\omega_{e2} \quad \omega_{e3}\omega_{e3})^T$.

The corresponding error dynamics is expressed as

$$I\dot{\boldsymbol{\omega}}_e = -k_2(\boldsymbol{\omega}_e - \boldsymbol{\xi}) - PG(\boldsymbol{\sigma})\boldsymbol{\sigma}_e + \boldsymbol{\tau}_d - \boldsymbol{\omega}^{\times}\Delta I\boldsymbol{\omega} - \Delta I\dot{\boldsymbol{\omega}}_d - \frac{\hat{\boldsymbol{\lambda}}_L * \boldsymbol{\omega}_e}{|\boldsymbol{\omega}_e| + \varepsilon_\lambda} \tag{17}$$

B. Optimal Coordinated Desaturation Controller

The required control torques can also be provided by the space tether:

$$\begin{aligned}\boldsymbol{\tau}_{c0}(k) &= \boldsymbol{\tau}_t(k) + \boldsymbol{\tau}_l(k)\\ &\boldsymbol{\tau}_t(k) + \left[R\left(\frac{[x,y,z]^T + R^{-1}\mathrm{d}}{\|[x,y,z]^T + R^{-1}\mathrm{d}\|}F_l(k)\right)\right]\times \mathrm{d}\\ &\boldsymbol{\tau}_t(k) + F_l(k)\boldsymbol{Q}(k)\end{aligned} \tag{18}$$

where $\boldsymbol{Q}(k) = \left[R\left(\frac{[x,y,z]^T+R^{-1}\mathrm{d}}{\|[x,y,z]^T+R^{-1}\mathrm{d}\|}F_l(k)\right)\right]\times \mathrm{d}$.

Equation (18) can be rewritten as

$$\boldsymbol{\tau}_{c0}(k) = C(k)\boldsymbol{\tau}(k) \tag{19}$$

where

$$C(k) = \begin{vmatrix}1 & 0 & 0 & \boldsymbol{Q}_1(k)\\ 0 & 1 & 0 & \boldsymbol{Q}_2(k)\\ 0 & 0 & 1 & \boldsymbol{Q}_3(k)\end{vmatrix}, \quad \boldsymbol{\tau}(k) = |\boldsymbol{\tau}_{t1}(k) \quad \boldsymbol{\tau}_{t2}(k) \quad \boldsymbol{\tau}_{t3}(k) \quad F_l(k)|^T$$

To obtain the optimal coordinated controllers, the following cost function is proposed:

$$J(k) = \frac{1}{2}\boldsymbol{\tau}(k)^T S\boldsymbol{\tau}(k) + \boldsymbol{\lambda}(k)^T(\boldsymbol{\tau}_{c0}(k) - C(k)\boldsymbol{\tau}(k)) \tag{20}$$

where $\boldsymbol{\lambda}(k) \in R^{3\times 1}$ are the Lagrange multipliers, and $S(k)$ is a constant positive weighting matrix that is used to decide the scalars of the thruster torques and tether tension.

Taking the derivatives of Eq. (20) with respect to $\boldsymbol{\tau}$ and $\boldsymbol{\lambda}$ yields

$$\boldsymbol{\tau}_{c0}(k) - C(k)\boldsymbol{\tau}(k) = 0 \tag{21}$$

$$\boldsymbol{\tau}(k)^T S - \boldsymbol{\lambda}(k)^T C(k) = 0 \tag{22}$$

Solving the preceding two equations, we have

$$\boldsymbol{\tau}(k) = S^{-1}C^T(k)(C(k)S^{-1}C^T(k))^{-1}\boldsymbol{\tau}_{c0}(k) \tag{23}$$

Figure 3 shows the block diagram of the coordinated attitude controller for the tethered space robot–target combination.

V. Numerical Simulation

Assuming that the $-V$-bar capture is adopted and the initial position of the combination is (200, 0, 0) m, the initial angular velocities of the three axes of the combination are $(8, -7, 9)$ deg/s. Table 1 shows the initial values of the parameters. Thrusters are assumed to have a constant control torque of 1 N · m when corresponding thrusters are turned on and work in PWM with a control cycle of 250 ms.

In this study, three controllers are simulated and the results are compared. The three controllers are 1) backstepping control (BC) without consideration of the thruster saturation and adaptation, 2) robust adaptive backstepping control (RABC) with consideration of the thruster saturation and adaptation in Eq. (14), and 3) coordinated robust adaptive backstepping control (CRABC) with consideration of the space tether tension, thruster saturation, and adaptation in Eqs. (14, 23). All the simulations are carried out in MATLAB 7.1 with a simulation step of 0.01 s, and the fourth-order Runge–Kutta method is used for integration.

Figure 4 provides the simulation results of the three-axis attitude $\boldsymbol{\sigma}_e$. From the comparisons in Fig. 4, one can observe that the attitude of the combination can be stabilized by BC, RABC, and CRABC. Compared with the other two controllers, with CRABC, the system states converge faster. Moreover, among these three methods, CRABC achieves the best transient performance with the smallest amplitudes and oscillations during the combination attitude stabilization. Figure 5 shows the response of the three-axis angular velocities of these three control methods.

Table 1 Initial value of the parameters

Parameters	Initial values
$\boldsymbol{\sigma}_e$	(0.2,0.2,0.2)
$\boldsymbol{\omega}_e$	$(8, -7, 9)$ deg/s
$[x \quad y \quad z]^T$	(200,0,0) m
$[\dot{x} \quad \dot{y} \quad \dot{z}]^T$	(0,0,0) m/s
n	0.0011 rad/s

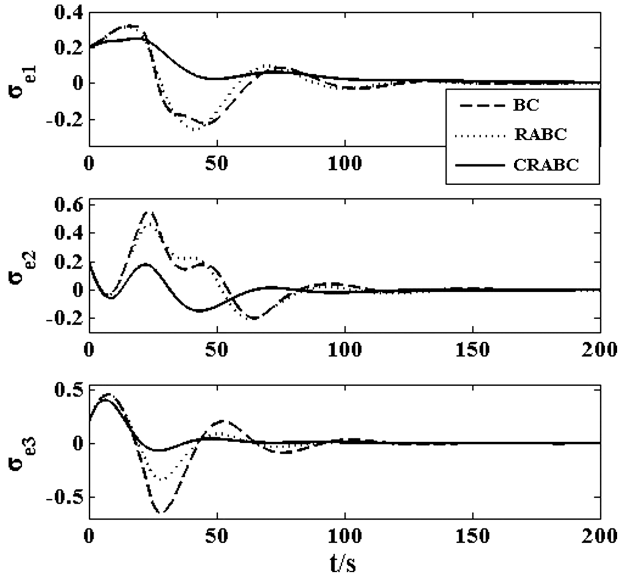

Fig. 4 Three-axis attitude σ_e of combination.

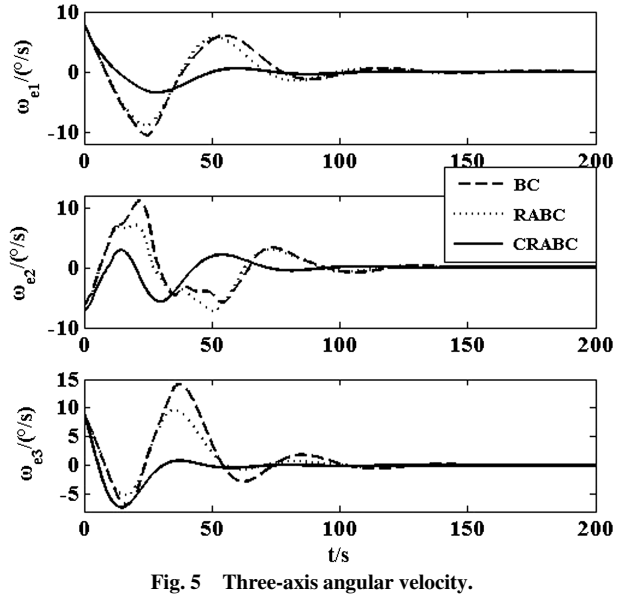

Fig. 5 Three-axis angular velocity.

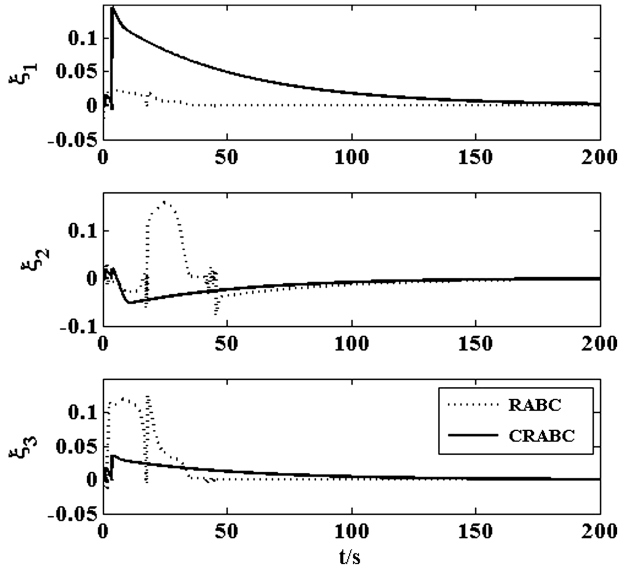

Fig. 6 ξ.

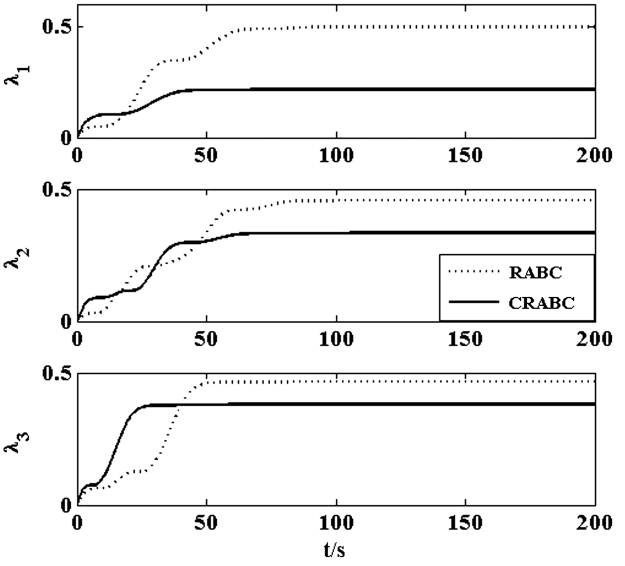

Fig. 7 Estimation values of λ_L.

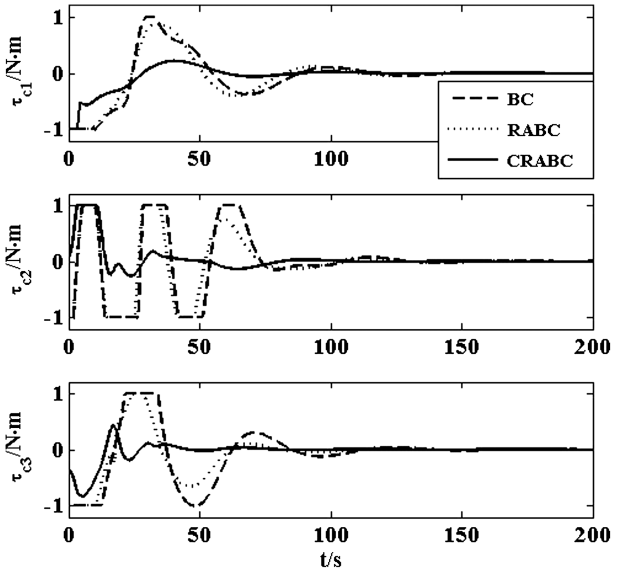

Fig. 8 Control torques of thrusters.

Figure 6 shows ξ, which are the states of the auxiliary design system for RABC and CRABC. Figure 7 shows the estimation values of λ_L. For RABC, the λ_L converges at (0.502,0.457,0.466), whereas estimation values for CRABC are (0.218,0.334,0.382).

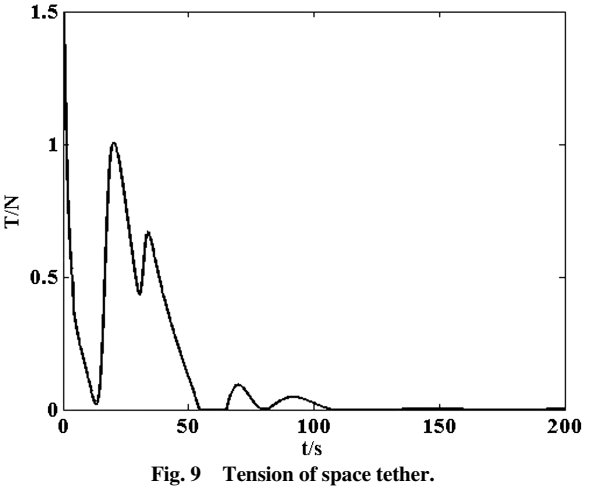

Fig. 9 Tension of space tether.

Figure 8 provides the thruster control torques of BC, RABC, and CRABC. It can be seen that $\Delta\boldsymbol{\tau}_c$ for RABC is obviously smaller than that of BC, which indicates that the utilization of the auxiliary design system is effective to desaturate the thrusters. Figure 9 is the corresponding tension along the space tether during the stabilization of the combinations.

VI. Conclusions

This Note presents a robust adaptive backstepping controller to achieve stabilization of a tumbling tethered space robot–target combination. The numerical simulations show that the combination can be stabilized by the proposed controller (CRABC). Compared with backstepping control and robust adaptive backstepping control, CRABC has the smallest saturation of the thrusters due to the utilization of the auxiliary design system and the optimal controller. Additionally, CRABC can realize the fastest attitude stabilization of the combination among these three controllers.

Appendix: Stability Analysis of Adaptive Controller

Choose the Lyapunov function as

$$W = W_1 + W_2 \tag{A1}$$

with $W_1 = \frac{1}{2}(\boldsymbol{\sigma}_e^T P \boldsymbol{\sigma}_e + \boldsymbol{y}^T \boldsymbol{y})$, and $W_2 = \frac{1}{2}\boldsymbol{\omega}_e^T I \boldsymbol{\omega}_e + \frac{1}{2a}\tilde{\boldsymbol{\lambda}}_L T \tilde{\boldsymbol{\lambda}}_L + \frac{1}{2}\boldsymbol{\xi}^T \boldsymbol{\xi}$.

According the definition of $\boldsymbol{y}$, the following equation can be obtained:

$$\dot{\boldsymbol{y}} = \dot{\boldsymbol{\omega}}_d - \dot{\boldsymbol{\omega}}_c = -\frac{\boldsymbol{y}}{\boldsymbol{\varepsilon}} + \boldsymbol{B}, \qquad \boldsymbol{B} = -\dot{\boldsymbol{\omega}}_c \tag{A2}$$

Assume the virtual control [Eq. (A2)] and its derivative are smooth bounded, and we know there exist constants $\boldsymbol{M}$ with $\boldsymbol{B} \le \boldsymbol{M}$.

Taking the derivative of W_1 yields

$$\begin{aligned}\dot{W}_1 &= \boldsymbol{\sigma}_e^T P \dot{\boldsymbol{\sigma}}_e + \boldsymbol{y}^T \dot{\boldsymbol{y}} \\ &= \boldsymbol{\sigma}_e^T P G(\boldsymbol{\sigma}) \boldsymbol{\omega}_e + \boldsymbol{\sigma}_e^T P G(\boldsymbol{\sigma}) \boldsymbol{y} - \boldsymbol{\sigma}_e^T P k_1 \boldsymbol{\sigma}_e - \frac{\boldsymbol{y}^T \boldsymbol{y}}{\boldsymbol{\varepsilon}} + \boldsymbol{y}^T \boldsymbol{B}\end{aligned} \tag{A3}$$

Because $\boldsymbol{B}$ is bounded, we have

$$\boldsymbol{y}^T \boldsymbol{B} \le \boldsymbol{y}^T \boldsymbol{y}/2 + \boldsymbol{B}^T \boldsymbol{B}/2 \le \boldsymbol{y}^T \boldsymbol{y}/2 + \boldsymbol{M}^T \boldsymbol{M}/2 \tag{A4}$$

According to the definition of $G(\boldsymbol{\sigma})$, we know $G(\boldsymbol{\sigma})$ is bounded. Therefore, the following equation can be obtained: $\|G(\boldsymbol{\sigma})\| \le \|G_M\|$. So, we have

$$\boldsymbol{\sigma}_e^T P \boldsymbol{G}(\boldsymbol{\sigma}) \boldsymbol{y} \le 0.5 \boldsymbol{\sigma}_e^T P \boldsymbol{G}_M \boldsymbol{\sigma}_e + 0.5 \boldsymbol{y}^T P \boldsymbol{G}_M \boldsymbol{y} \tag{A5}$$

Substituting Eqs. (A4) and (A5) into Eq. (A3), we have

$$\begin{aligned}\dot{W}_1 &\le \boldsymbol{\sigma}_e^T P G(\boldsymbol{\sigma}) \boldsymbol{\omega}_e + 0.5 \boldsymbol{\sigma}_e^T P G_M \boldsymbol{\sigma}_e + 0.5 \boldsymbol{y}^T P G_M \boldsymbol{y} - \boldsymbol{\sigma}_e^T P k_1 \boldsymbol{\sigma}_e \\ &\quad - \frac{\boldsymbol{y}^T \boldsymbol{y}}{\boldsymbol{\varepsilon}} + 0.5 \boldsymbol{M}^T \boldsymbol{M} + 0.5 \boldsymbol{y}^T \boldsymbol{y} \\ &= \boldsymbol{\sigma}_e^T P G(\boldsymbol{\sigma}) \boldsymbol{\omega}_e - \boldsymbol{\sigma}_e^T P k_1 \boldsymbol{\sigma}_e + 0.5 \boldsymbol{\sigma}_e^T P G_M \boldsymbol{\sigma}_e \\ &\quad + 0.5 \boldsymbol{M}^T \boldsymbol{M} + \boldsymbol{y}^T \left(0.5 P G_M - \frac{1}{\boldsymbol{\varepsilon}} + 0.5 \right) \boldsymbol{y}\end{aligned} \tag{A6}$$

Taking the derivative of W_2 yields

$$\begin{aligned}\dot{W}_2 &= \boldsymbol{\omega}_e^T I \dot{\boldsymbol{\omega}}_e + \frac{1}{a} \tilde{\boldsymbol{\lambda}}_L^T \dot{\tilde{\boldsymbol{\lambda}}}_L + \boldsymbol{\xi}^T \dot{\boldsymbol{\xi}} \\ &= -\boldsymbol{\omega}_e^T k_2 \boldsymbol{\omega}_e + \boldsymbol{\omega}_e^T k_2 \boldsymbol{\xi} - \boldsymbol{\omega}_e^T P G(\boldsymbol{\sigma}) \boldsymbol{\sigma}_e - \frac{\hat{\boldsymbol{\lambda}}_L^T (\boldsymbol{\omega}_e * \boldsymbol{\omega}_e)}{|\boldsymbol{\omega}_e| + \varepsilon_\lambda} \\ &\quad + \boldsymbol{\omega}_e^T (-\boldsymbol{\omega}^{\times} \Delta I \boldsymbol{\omega} - \Delta I \dot{\boldsymbol{\omega}}_d + \boldsymbol{\tau}_d) + \frac{\tilde{\boldsymbol{\lambda}}_L^T (\boldsymbol{\omega}_e * \boldsymbol{\omega}_e)}{|\boldsymbol{\omega}_e| + \varepsilon_\lambda} \\ &\quad - \boldsymbol{\xi}^T K_\xi \boldsymbol{\xi} - \boldsymbol{\xi}^T \frac{|\boldsymbol{\omega}_e^T \Delta \boldsymbol{T}_c| + 0.5 \Delta \boldsymbol{T}_c^T \Delta \boldsymbol{T}_c}{\|\boldsymbol{\xi}\|^2} \boldsymbol{\xi} + \boldsymbol{\xi}^T \Delta \boldsymbol{\tau}_c \\ &\le -0.5 \boldsymbol{\omega}_e^T k_2 \boldsymbol{\omega}_e - \boldsymbol{\omega}_e^T P G(\boldsymbol{\sigma}) \boldsymbol{\sigma}_e - \frac{\boldsymbol{\lambda}_L^T (\boldsymbol{\omega}_e * \boldsymbol{\omega}_e)}{|\boldsymbol{\omega}_e| + \varepsilon_\lambda} \\ &\quad + |\boldsymbol{\omega}_e^T| |\boldsymbol{\lambda}_L| - |\boldsymbol{\omega}_e^T \Delta \boldsymbol{\tau}_c| + \boldsymbol{\xi}^T (0.5 - K_\xi - 0.5 k_2) \boldsymbol{\xi}\end{aligned} \tag{A7}$$

Combining $\dot{W}_1$ and $\dot{W}_2$, we have

$$\begin{aligned}\dot{W} &\le \boldsymbol{\sigma}_e^T P G(\boldsymbol{\sigma}) \boldsymbol{\omega}_e - \boldsymbol{\sigma}_e^T P k_1 \boldsymbol{\sigma}_e + 0.5 \boldsymbol{\sigma}_e^T P G_M \boldsymbol{\sigma}_e \\ &\quad + 0.5 \boldsymbol{M}^T \boldsymbol{M} + \boldsymbol{y}^T \left(0.5 P G_M - \frac{1}{\boldsymbol{\varepsilon}} + 0.5 \right) \boldsymbol{y} \\ &\quad - 0.5 \boldsymbol{\omega}_e^T k_2 \boldsymbol{\omega}_e - \boldsymbol{\omega}_e^T P G(\boldsymbol{\sigma}) \boldsymbol{\sigma}_e - \frac{\boldsymbol{\lambda}_L^T \boldsymbol{\omega}_e^2}{|\boldsymbol{\omega}_e| + \varepsilon_\lambda} \\ &\quad + |\boldsymbol{\omega}_e^T| |\boldsymbol{\lambda}_L| - |\boldsymbol{\omega}_e^T \Delta \boldsymbol{\tau}_c| + \boldsymbol{\xi}^T (0.5 - K_\xi - 0.5 k_2) \boldsymbol{\xi} \\ &\quad \boldsymbol{\sigma}_e^T P (0.5 G_M - \boldsymbol{k}_1) \boldsymbol{\sigma}_e + 0.5 \boldsymbol{M}^T \boldsymbol{M} + \boldsymbol{y}^T \left(0.5 P G_M - \frac{1}{\boldsymbol{\varepsilon}} + 0.5 \right) \boldsymbol{y} \\ &\quad - 0.5 \boldsymbol{\omega}_e^T k_2 \boldsymbol{\omega}_e + \left(-\frac{\boldsymbol{\lambda}_L^T \boldsymbol{\omega}_e^2}{|\boldsymbol{\omega}_e| + \varepsilon_\lambda} + |\boldsymbol{\omega}_e^T| |\boldsymbol{\lambda}_L| \right) - |\boldsymbol{\omega}_e^T \Delta \boldsymbol{\tau}_c| \\ &\quad + \boldsymbol{\xi}^T (0.5 - K_\xi - 0.5 k_2) \boldsymbol{\xi}\end{aligned} \tag{A8}$$

where $-(\lambda_L^T \boldsymbol{\omega}_e^2 / |\boldsymbol{\omega}_e| + \varepsilon_\lambda) + |\boldsymbol{\omega}_e^T| |\lambda_L| \le 0$

It can be seen that, when $0.5\boldsymbol{G}_M - k_1$, $0.5 - K_\xi - 0.5 k_2$, and $0.5 P \boldsymbol{G}_M - (1/\boldsymbol{\varepsilon}) + 0.5$ are positive-definite matrices, the closed-system stability is uniformly, ultimately bounded according to the Lassalle–Yoshizawa theorem.

Acknowledgments

This research is sponsored by the National Natural Science Foundation of China (grant nos. 11272256 and 61005062).

References

[1] Cartmell, M. P., and McKenzie, D. J., "A Review of Space Tether Research," *Progress in Aerospace Sciences*, Vol. 44, No. 1, 2008, pp. 1–21.
doi:10.1016/j.paerosci.2007.08.002

[2] Kumar, K. D., "Review of Dynamics and Control of Nonelectrodynamic Tethered Satellite Systems," *Journal of Spacecraft and Rockets*, Vol. 43, No. 4, 2006, pp. 705–720.
doi:10.2514/1.5479

[3] Williams, P., "In-Plane Payload Capture with an Elastic Tether," *Journal of Guidance, Control, and Dynamics*, Vol. 29, No. 4, 2006, pp. 810–821.
doi:10.2514/1.17474

[4] Zhai, G., Qiu, Y., Liang, B., and Li, C., "On-Orbit Capture with Flexible Tether–Net System," *Acta Astronautica*, Vol. 65, No. 5, 2009, pp. 613–623.
doi:10.1016/j.actaastro.2009.03.011

[5] Nohmi, M., "Mission Design of a Tethered Robot Satellite 'STARS' for Orbital Experiment," *IEEE Control Applications, (CCA) and Intelligent Control (ISIC)*, IEEE, Piscataway, NJ, 2009, pp. 1075–1080.
doi:10.1109/CCA.2009.5281113

[6] Godard, , Kumar, K. D., and Tan, B., "Nonlinear Optimal Control of Tethered Satellite Systems Using Tether Offset in the Presence of Tether Failure," *Acta Astronautica*, Vol. 66, No. 9, 2010, pp. 1434–1448.
doi:10.1016/j.actaastro.2009.10.037

[7] Bergamaschi, S., and Bonon, F., "Coupling of Tether Lateral Vibration and Sub-Satellite Attitude Motion," *Journal of Guidance, Control, and Dynamics*, Vol. 15, No. 5, 1992, pp. 1284–1286.

[8] Wang, D., Huang, P., Cai, J., and Meng, Z., "Coordinated Control of Tethered Space Robot Using Mobile Tether Attachment Point in Approaching Phase," *Advances in Space Research*, Vol. 54, No. 6, 2014, pp. 1077–1091.
doi:10.1016/j.asr.2014.05.016

[9] Yoshida, K., Dimitar, D., and Hiroki, N., "On the Capture of Tumbling Satellite by a Space Robot," *2006 IEEE/RSJ International Conference on IEEE Intelligent Robots and Systems*, IEEE, Piscataway, NJ, 2006, pp. 4127–4132.
doi:10.1109/IROS.2006.281900

[10] Flores-Abad, A. and , and Ma, O., "Control of a Space Robot for Minimal Attitude Disturbance to the Base Satellite for Capturing a Tumbling Satellite," *Proceedings of the SPIE: Sensors and Systems for Space Applications*, Vol. 8385, SPIE, Bellingham, WA, 2012, Paper 83850J.
doi:10.1117/12.918523

[11] Liu, S., Licheng, W., and Zhen, L., "Impact Dynamics and Control of a Flexible Dual-Arm Space Robot Capturing an Object," *Applied Mathematics and Computation*, Vol. 185, No. 2, 2007, pp. 1149–1159.
doi:10.1016/j.amc.2006.07.035

[12] Aghili, F., "Optimal Control of a Space Manipulator for Detumbling of a Satellite," *International Conference on Robotics and Automation*, IEEE, Piscataway, NJ, May 2009, pp. 3019–3024.
doi:10.1109/ROBOT.2009.5152235

[13] Xu, W., Cheng, L., Liang, B., Xu, Y., Liu, Y., and Qiang, W., "Target Berthing and Base Reorientation of Free-Floating Space Robotic System After Capturing" *Acta Astronautica*, Vol. 64, Nos. 2–3, 2009, pp. 109–126.
doi:10.1016/j.actaastro.2008.07.010

[14] Huang, P., Wang, D., Meng, Z., and Liu, Z., "Post-Capture Attitude Control for a Tethered Space Robot–Target Combination System," *Robotica* [online], March 2014, pp. 1–22.
doi:10.1017/S0263574714000617

[15] Chen, M., Ge, S., and How, B., "Robust Adaptive Neural Network Control for a Class of Uncertain MIMO Nonlinear Systems with Input Nonlinearities," *IEEE Transactions on Neural Networks*, " Vol. 21, No. 5, 2010, pp. 796–812.
doi:10.1109/TNN.2010.2042611

[16] Xu, B., Huang, X., Wang, D., and Sun, F., "Dynamic Surface Control of Constrained Hypersonic Flight Models with Parameter Estimation and Actuator Compensation," *Asian Journal of Control* [online], Vol. 16, No. 1, 2014, pp. 162–174.
doi:10.1002/asjc.679

[17] Xia, G., et al., "Adaptive Neural Network Control with Backstepping for Surface Ships with Input Dead-Zone," *Mathematical Problems in Engineering*, Vol. 2013, 2013.
doi:10.1155/2013/530162

[18] Wen, C., Zhou, J., Liu, Z., and Su, H., "Robust Adaptive Control of Uncertain Nonlinear Systems in the Presence of Input Saturation and External Disturbance," *IEEE Transactions on Automatic Control*, Vol. 56, No. 7, 2011, pp. 1672–1678.
doi:10.1109/TAC.2011.2122730

[19] Crassidis, J. L., and Markley, F. L., "Sliding Mode Control Using Modified Rodrigues Parameters," *Journal of Guidance, Control, and Dynamics*, Vol. 19, No. 6, 1996, pp. 1381–1383.
doi:10.2514/3.21798